

https://doi.org/10.1070/QEL17592

Q-switched lasing in $ZrO_2-Y_2O_3-Ho_2O_3$ crystals

S.A. Artemov, E.A. Artemov, E.E. Lomonova, P.A. Ryabochkina, A.N. Chabushkin

Abstract. **The energy and time characteristics of *Q*-switched two-micron lasing at the $^5I_7 \rightarrow {}^5I_8$ transition of Ho^{3+} ions in $ZrO_2-Y_2O_3-Ho_2O_3$ crystals are studied under resonance pumping to the $^5I_7$ level by a cw $Tm:LiYF_4$ laser. The mechanisms of appearance of burns on the faces of the $ZrO_2-Y_2O_3-Ho_2O_3$ active elements at high laser energy densities are proposed.**

Keywords: *$ZrO_2-Y_2O_3-Ho_2O_3$ crystals, two-micron lasing, Q-switched regime.*

1. Introduction

At present, there exit two-micron solid-state lasers based on active crystals, glasses, and ceramics doped with Tm^{3+} or Ho^{3+} ions. Nevertheless, search for new active media for this spectral region still continues. This is explained, first of all, by practical application of two-micron lasers in medicine, for monitoring of various gases, in lidar systems, and for pumping of lasers emitting in the spectral range of 4–5 μm. The results of investigations aimed at the development of two-micron lasers based on various crystals and ceramics doped with Tm^{3+} or Ho^{3+} are published in [1–21].

Previously, we reported about obtaining two-micron lasing at the $^5I_7 \rightarrow {}^5I_8$ transition of Ho^{3+} ions in $ZrO_2-Y_2O_3-Ho_2O_3$ crystals under resonance pumping of these ions into the $^5I_7$ level by cw solid-state $Tm:LiYF_4$ [17, 19] and thulium fibre [20] lasers, as well as by a pulsed $Tm:LiYF^4$ laser [21].

A specific feature of $ZrO_2-Y_2O_3$ crystals doped with rare-earth (RE) ions is that the crystal field splitting of multiplets of RE ions in these crystals [like in sesquioxide crystals and ceramics (Y_2O_3, Lu_2O_3, Sc_2O_3) doped with RE ions] is stronger than in other oxide materials (for example, in $Y_3A_{l5}O_{12}$) [18]. In particular, the luminescence spectrum of the $^5I_7 \rightarrow {}^5I_8$ transition of Ho^{3+} ions in $ZrO_2-Y_2O_3-Ho_2O_3$ crystals lies in the range of 1800–2300 nm. This made it possible to obtain lasing in these crystals at the longest wavelengths compared to the other Ho^{3+}-doped crystals and achieve wavelength tuning in the range of 2056–2168 nm [19].

S.A. Artemov, P.A. Ryabochkina N.P. Ogarev Mordovian State University, ul. Bol'shevistskaya 68, 430005 Saransk, Russia; e-mail: ryabochkina@freemail.mrsu.ru;
E.A. Artemov, E.E. Lomonova Prokhorov General Physics Institute, Russian Academy of Sciences, ul. Vavilova 38, 119991 Moscow, Russia;
A.N. Chabushkin International Center of Quantum Optics and Quantum Technologies, ul. Novaya 100, 143026 Skolkovo, Moscow region, Russia

Received 26 May 2021
Kvantovaya Elektronika **51** (7) 586–592 (2021)
Translated by M.N. Basieva

In [20], we obtained two-micron lasing at the $^5I_7 \rightarrow {}^5I_8$ transition of Ho^{3+} ions in $ZrO_2-Y_2O_3-Ho_2O_3$ crystals in the *Q*-switched regime under pumping by a cw thulium fibre laser into the $^5I_7$ level of Ho^{3+}. The laser pulse duration was 140 and 310 ns at pulse repetition rates of 1 and 10 kHz, respectively. However, detailed studies of the energy and time characteristics of *Q*-switched lasing in $ZrO_2-Y_2O_3-Ho_2O_3$ crystals were not performed in [20] due the appearance of characteristic burns on the faces of the active elements (AEs).

The present work continues the series of investigations of the laser characteristics of $ZrO_2-Y_2O_3-Ho_2O_3$ crystals. The aim of this work is to study in detail the time and energy characteristics of *Q*-switched lasing upon pumping by a cw $Tm:LiYF_4$ laser and to reveal the reasons for the appearance of burns on the AE faces with decreasing the laser pulse duration.

2. Experimental

We studied $ZrO_2-Y_2O_3$(13.4 mol%)$-Ho_2O_3$(0.6 mol%) crystals grown by direct high-frequency heating in a cold container 130 mm in diameter in a Kristall-407 crystal-growth furnace at a crucible lowering rate of 10 mm h^{-1}. A decrease in the growth rate of zirconia-based crystals led to a decrease in the number of optical defects called growth bands [22], which cause losses in AEs [23]. For laser experiments, we cut from these crystals AEs in the form of rectangular parallelepipeds $3 \times 3 \times 20$ mm in size.

To clarify the reasons for the appearance of burns on the AE faces with increasing laser power density [20], we used different treatment methods, including chemical-mechanical polishing (CMP). To exclude the influence of antireflection coatings on the appearance of burn, the laser experiments on $ZrO_2-Y_2O_3-Ho_2O_3$ crystals in this work (in contrast to [20]) were performed using elements without antireflection coatings on faces.

We performed two series of experiments with AEs made of $ZrO_2-Y_2O_3$(13.4 mol%)$-Ho_2O_3$(0.6 mol%) crystals; the growth rates and the methods of treatment of faces are presented in Table 1.

Figure 1 shows the spectral dependences of absorption ($^5I_8 \rightarrow {}^5I_7$) and stimulated emission ($^5I_7 \rightarrow {}^5I_8$) cross sections of Ho^{3+} ions in $ZrO_2-Y_2O_3-Ho_2O_3$ crystals, which were previously obtained in our works [18–21] from experimentally recorded absorption and luminescence spectra of Ho^{3+} ions ($^5I_8 \rightarrow {}^5I_7$ and $^5I_7 \rightarrow {}^5I_8$ transitions, respectively). The absorption cross section spectrum indicates that the wavelength 1910 nm is optimal for pumping into the $^5I_7$ level to obtain lasing at the $^5I_7 \rightarrow {}^5I_8$ transition of Ho^{3+} ions.

Table 1. Parameters of active elements cut from ZrO_2–Y_2O_3(13.4 mol%)–Ho_2O_3(0.6 mol%) crystals.

Series number	AE number	Crystal growth rate V/mm h^{-1}	Treatment before CMP	Annealing conditions*	CMP time/min
1	1	4	AM**	Exposure at 2100 °C in vacuum/10^{-3}–10^{-4} mm Hg for 1–2 h and cooling with a rate of 80 °C h^{-1}	10
	2	4	AM		10
	3	4	AM		10
2	4	4	AM		10
	5	10	AM		20
	6	10	AM → annealing → AM		30

*Annealing time depended on the crystal size and decreased to 1 h for small crystals;

**AM means mechanical treatment with diamond abrasive with a grain size of 1 μm.

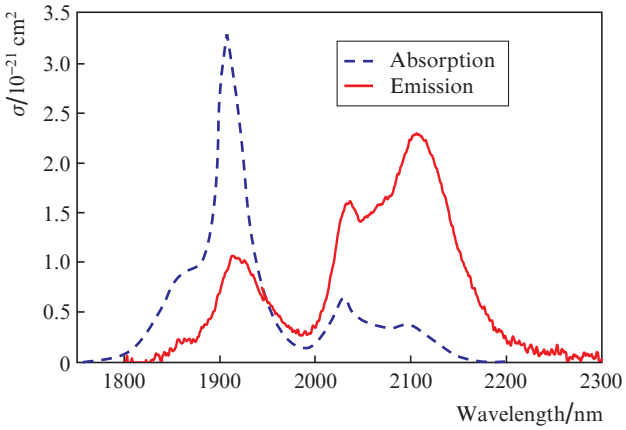

Figure 1. Spectral dependences of the $^5I_8 \rightarrow {}^5I_7$ absorption and $^5I_7 \rightarrow {}^5I_8$ stimulated emission cross sections of Ho^{3+} ions for ZrO_2–Y_2O_3–Ho_2O_3 crystals at $T = 300$ K [18–21].

Optical scheme 1 of a two-micron ZrO_2–Y_2O_3–Ho_2O_3 laser Q-switched by an acousto-optic Q-switch, which was used in the first series of laser experiments, is shown in Fig. 2. Ho^{3+} ions in ZrO_2–Y_2O_3–Ho_2O_3 crystals were pumped into the $^5I_7$ level by a cw Tm:$LiYF_4$ laser with a wavelength of 1910 nm and a maximum output power of 7.5 W. The pump radiation was focused into active element 1 using a two-lens objective; the beam waist diameter was 320 μm.

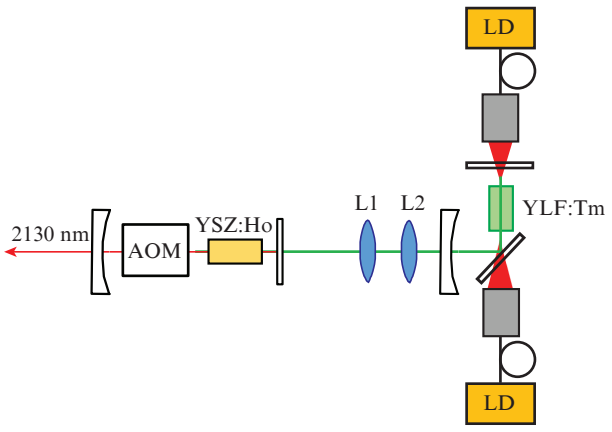

Figure 2. Optical scheme 1 of a Q-switched two-micron laser based on the $^5I_7 \rightarrow {}^5I_8$ transition of Ho^{3+} ions in ZrO_2–Y_2O_3–Ho_2O_3 (YSZ:Ho) crystals: (LD) laser diode; (L1 and L2) lenses; (AOM) acousto-optic modulator.

The laser cavity 80 mm long was formed by a plane input mirror with transmission coefficients $\mathcal{T} = 93\%$ at the pump wavelength (1910 nm) and $\mathcal{T} = 0.1\%$ at the lasing wavelength (2130 nm) and by a spherical output mirror with a radius of curvature of 150 mm and transmission coefficient $\mathcal{T} = 6\%$ at the lasing wavelength. For Q-switching, an acousto-optic modulator made of a quartz crystal was placed in front of the spherical output mirror.

To perform laser experiments, the studied active elements were wrapped in indium foil and mounted in a copper holder.

The laser signal was recorded by a PDA10D2 (Thorlabs) photodetector. The laser pulse duration and repetition rate were measured with a Tektronix TDS 2022C digital oscilloscope. The output laser power was measured using a Thorlabs S405C power meter. The laser spectra were recorded on a AQ6375B (Yokogawa) optical spectrum analyser.

The upconversion luminescence spectrum of ZrO_2–Y_2O_3–Ho_2O_3 crystals excited by a thulium fibre laser with a wavelength of 1940 nm was recorded using a spectrometer based on an FHR 1000 (Horiba) monochromator. The luminescence was recorded by an R928 PMT (Hamamatsu).

The excitation spectrum of ZrO_2–Y_2O_3–Ho_2O_3 crystals in the range of 220–540 nm was recorded by an RF-5301 PC (Shimadzu) spectrofluorimeter with a xenon lamp as an excitation source.

3. Experimental results and discussion

Pumping of AE 1 by radiation with a power of 3 W led to lasing of Ho^{3+} ions at the $^5I_7 \rightarrow {}^5I$ transition in the Q-switched regime with a pulse duration of 300 ns and a pulse repetition rate of 1 kHz. The laser spectrum in the Q-switched regime for this AE is shown in Fig. 3a, and Fig. 3b presents the laser spectrum in the cw regime for comparison. One can see that the spectrum of the pulsed radiation is shifted to shorter wavelengths with respect of the spectrum in the cw regime, which is caused by an enhanced population inversion in the case of the Q-switched regime and correlates with the spectral dependence of the gain cross section for ZrO_2–Y_2O_3–Ho_2O_3 crystals given in [17, 20].

Figure 4 presents the dependences of the cw output laser power on the incident pump power for AEs 1–3. One can see that the slope laser efficiencies η for these AEs differ only slightly and lie within the range 28%–33%.

For AEs 1–3, Figs 5a and 5b show the dependences of the average and peak output laser power on the pump power at a pulse repetition rate of 1 kHz, while the dependence of the laser pulse duration on the pump power is shown in Fig. 5c. These figures reveal that the laser parameters (pulse duration

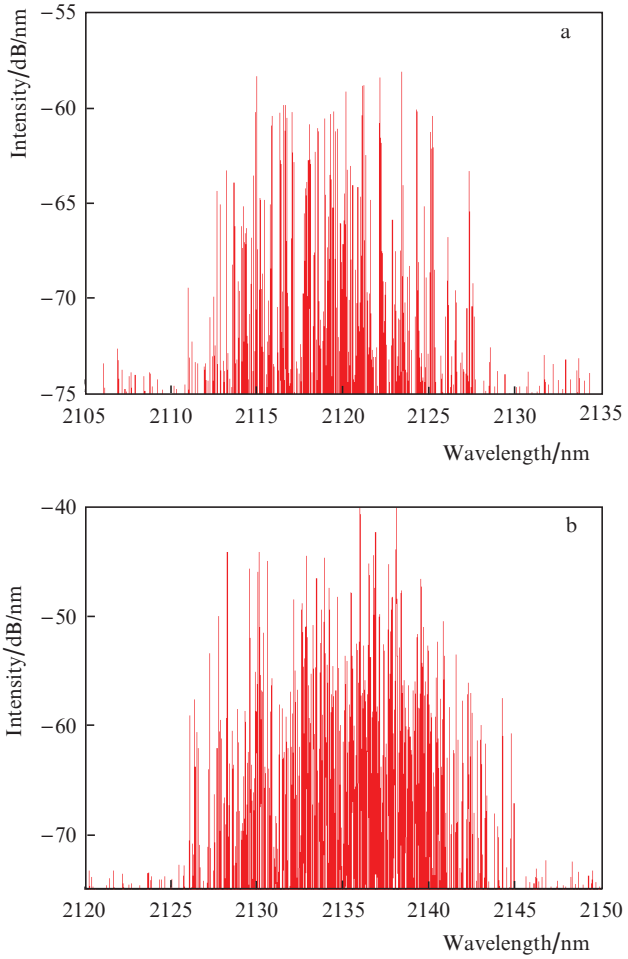

Figure 3. Laser spectra for the $^5I_7 \rightarrow {}^5I_8$ transition of Ho^{3+} ions in AE 1 in (a) *Q*-switched and (b) cw regimes.

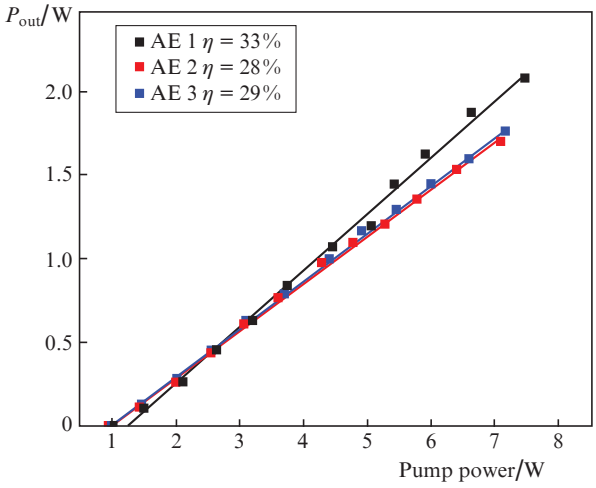

Figure 4. (Colour online) Dependences of the output laser power at the $^5I_7 \rightarrow {}^5I_8$ transition of Ho^{3+} ions on the incident pump power for AEs 1–3.

and output power) in the *Q*-switched regime (like in the case of cw lasing) for AEs 1–3 differ insignificantly.

The oscillogram of a shortest pulse and a typical train of pulses at a pulse repetition rate of 1 kHz obtained in the experiment with AE 1 are shown in Fig. 6. The amplitudes of pulses in the train somewhat differ from each other. We

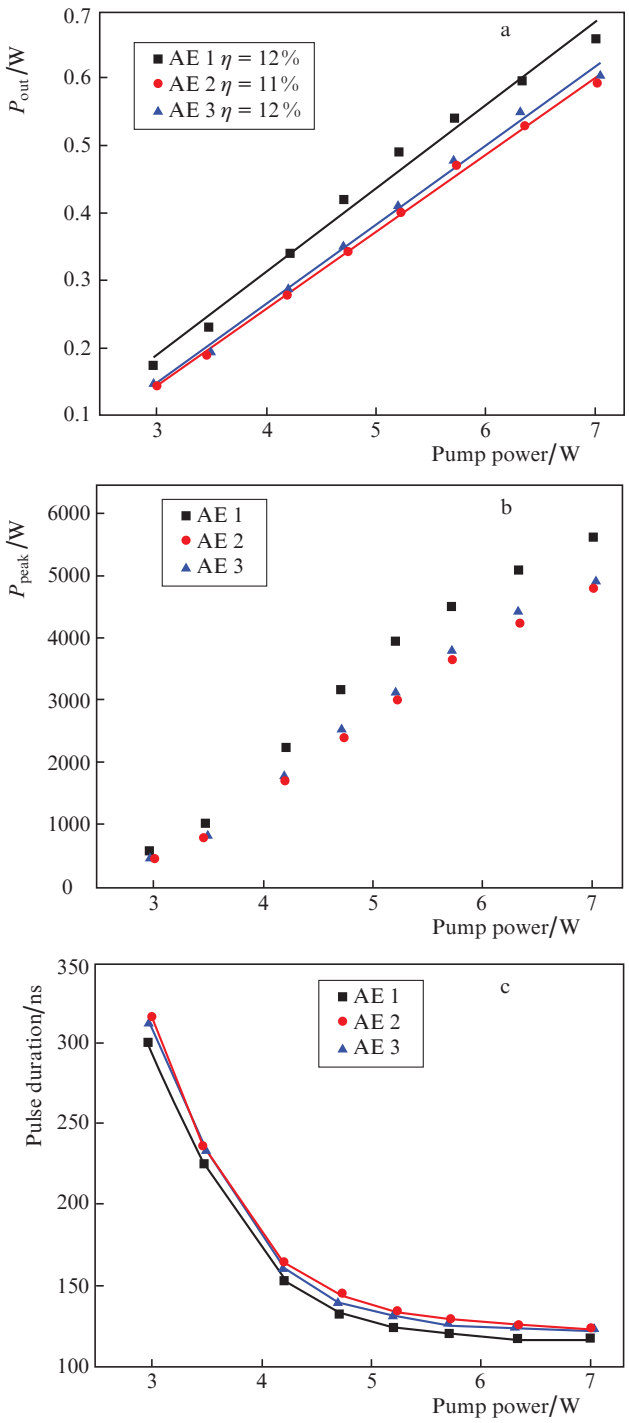

Figure 5. (Colour online) Dependences of the (a) average and (b) peak pulsed output power of lasing at the $^5I_7 \rightarrow {}^5I_8$ transition of Ho^{3+} ions in the *Q*-switched regime on the incident pump power for AEs 1–3, as well as (c) dependences of the laser pulse duration on the pump power. Pulse repetition rate 1 kHz.

believe that this can be related to the multimode lasing regime under the condition that the pump spot size is larger than the size of the cavity mode inside the active element. Since the transverse intensity distributions of laser modes are different, the contributions of different modes to the generated power in the case of *Q*-switching will be different due to, in particular, a change in the population inversions of modes from pulse to pulse.

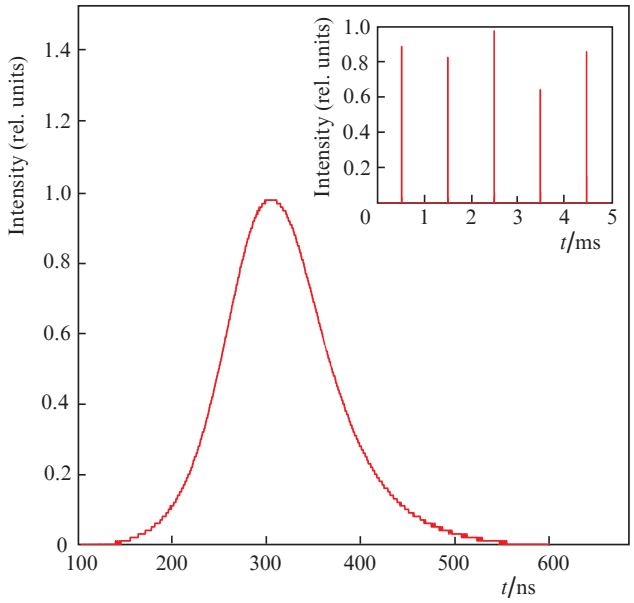

Figure 6. Oscillogram of a pulse with the shortest duration and typical train of pulses at a repetition rate of 1 kHz for AE 1.

Focusing of pump radiation on different regions of the faces of AEs in the first series of laser experiments revealed regions in which the laser operation at a pulse repetition rate of 1 kHz was stable up to the maximum pump powers. At the same time, the AE faces had regions with burns formed with increasing the pump power and, hence, the lasing power density. Figure 7 shows the images of typical burns obtained using an Axio Imager Z2 Vario (Carl Zeiss) high-resolution optical microscope. It should be noted that these burns appeared only on the surfaces of the AEs, while volume breakdowns were not observed.

To determine the influence of the crystal growth conditions and the AE surface treatment quality on the appearance of burns, we performed the second series of experiments with AEs 4, 5, and 6 (Table 1). AE 4 was cut from a crystal that was grown with a rate of 4 mm h^{-1} and then annealed in vacuum for 1 h at $T = 1400\,^{\circ}C$ before CMP. Active elements 5 and 6 were cut from a crystal grown with a rate of 10 mm h^{-1}; the crystal for AE 5 was also annealed in vacuum for 1 h at $T = 1400\,^{\circ}C$, while the crystal for AE 6 after annealing in vacuum was mechanically polished, annealed again, and once more mechanically polished before CMP. The CMP duration for AEs 4, 5, and 6 was 10, 20, and 30 min, respectively.

Experiments with AEs 4–6 were performed using optical scheme 1 (see Fig. 2). The cavity parameters and the pump beam waist diameter were similar to those used in the first series of laser experiments. The maximum pump power was 5.1 W.

The dependences of the average and peak output powers of pulsed laser radiation on the pump power for AEs 4–6, as well as the dependences of the laser pulse duration on the pump power at a pulse repetition rate of 1 kHz are presented in Fig. 8.

One can see from Fig. 8 that the best energy characteristics and the shortest pulse duration are demonstrated by AE 4, which was cut from the ZrO_2–Y_2O_3(13.4 mol%)–Ho_2O_3(0.6 mol%) crystal grown with a rate of 4 mm h^{-1} and whose faces were chemically and mechanically polished for 10 min. The oscillogram of the shortest pulse and a typical train of pulses with a repetition rate of 1 kHz for AE 4 are given in Fig. 9.

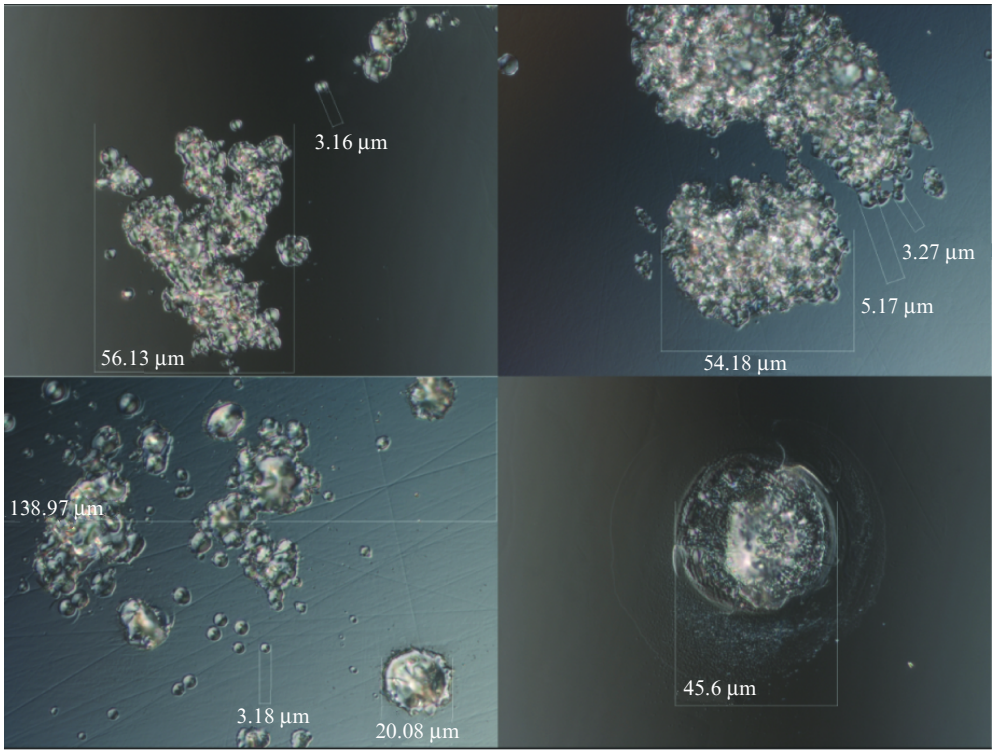

Figure 7. (Colour online) Images of burns on the face of an active element after the laser experiment obtained using an Axio Imager Z2 Vario microscope.

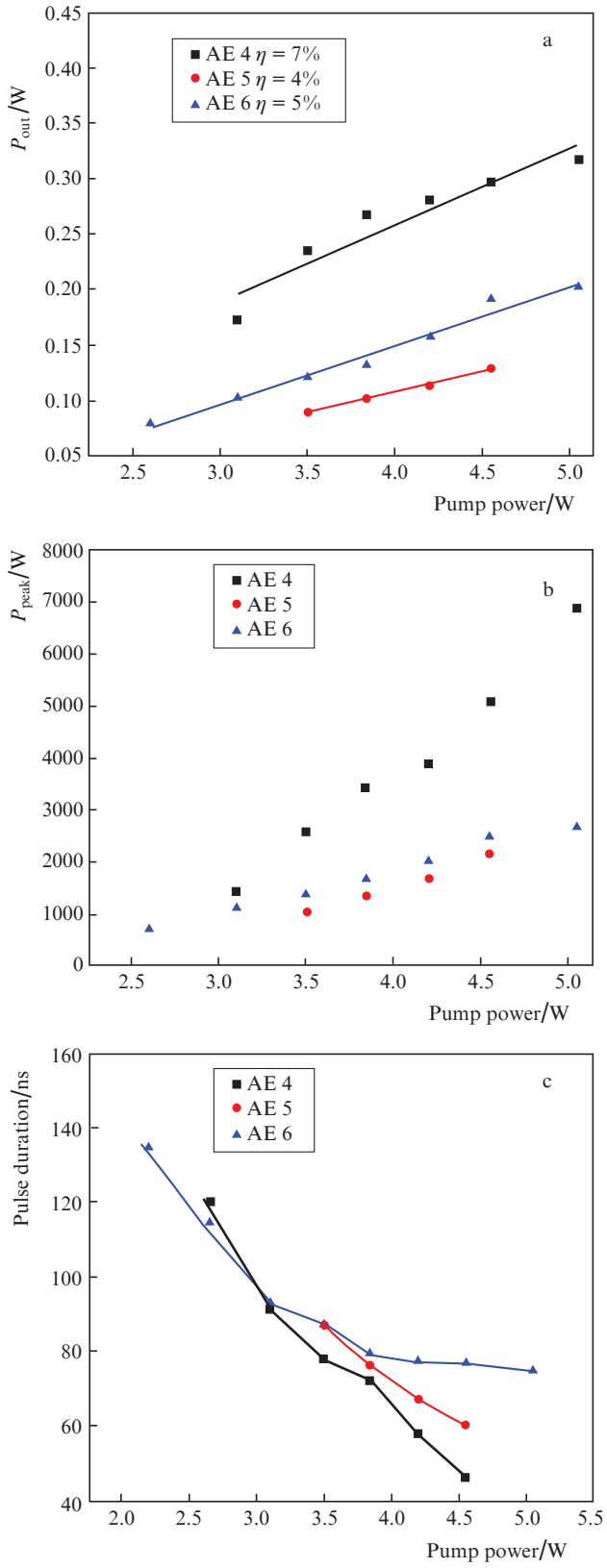

Figure 8. (Colour online) Dependences of the (a) average and (b) peak pulsed output power of lasing at the $^5I_7 \rightarrow {}^5I_8$ transition of Ho^{3+} ions; as well as (c) dependences of laser pulse duration on the incident pump power for AEs 4–6. The pulse repetition rate is 1 kHz.

Note that, similar to the first series of experiments with AEs 1–3, an increase in the pump power and in the laser

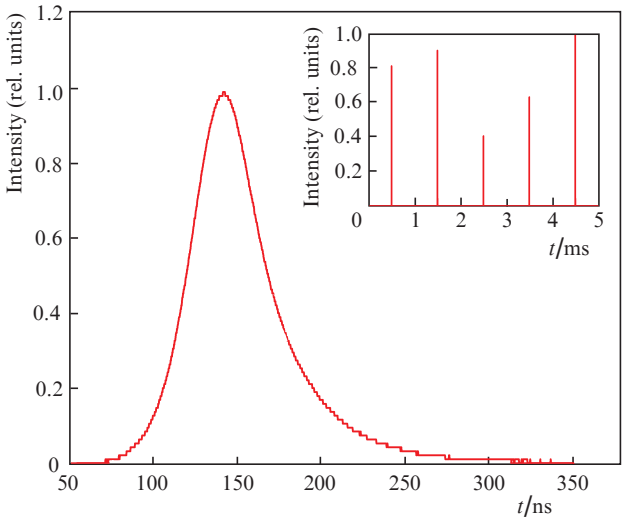

Figure 9. Oscillogram of a pulse with the shortest duration and typical train of pulses at a pulse repetition rate of 1 kHz for AE 4.

power density caused the appearance of burns in some regions of faces of AEs 4–6.

An additional experiment, whose optical scheme is presented in Fig. 10, was performed with AE 4, which is characterised by the best energy characteristics and the shortest pulse duration. Scheme 2 contained an additional plane dichroic mirror inclined at an angle of 45° to the cavity axis, which had a transmission coefficient of 98% at the pump wavelength and a reflection coefficient of 100% at the lasing wavelength and was installed to minimize the pump radiation

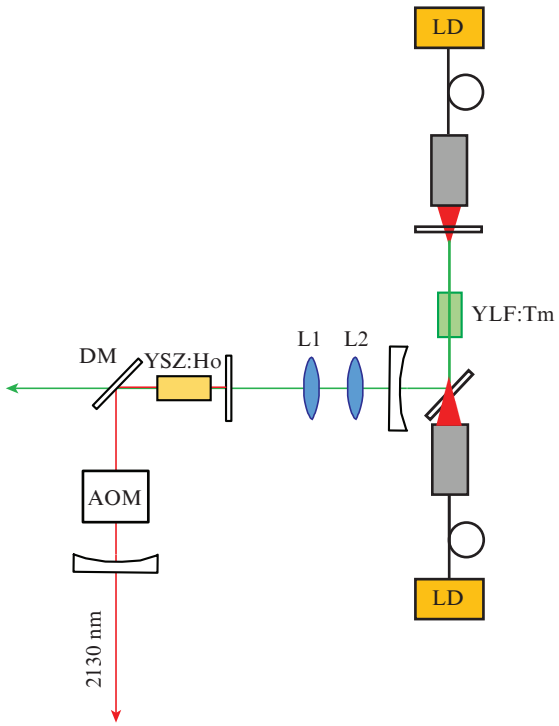

Figure 10. Optical scheme 2 of a two-micron laser based on ZrO_2–Y_2O_3–Ho_2O_3 crystals: (DM) dichroic mirror (the other designations are the same as in Fig. 2).

incident on the rear face of the AE. The cavity length in this case was 92 mm.

The use of optical scheme 2 did not allow us to avoid the appearance of burns and led only to an increase in the pulse duration to 85 ns at a pulse repetition rate of 1 kHz and a pump power of 4.5 W (versus 46 ns obtained in scheme 1).

Thus, both series of experiments on *Q*-switched lasing in AEs made of ZrO_2–Y_2O_3–Ho_2O_3 crystals showed that an increase in the lasing power density and a decrease in the laser pulse duration cause the appearance of characteristic burns on the faces of active elements.

One of the reasons for the appearance of burns can be related to the structure of these crystals, which is characterised by the existence of oxygen vacancies formed due the necessity of charge compensation in the case of heterovalent substitution of Zr^{4+} cations by Yb^{3+} and RE ions. Anion vacancies with captured electrons can have energy levels near the conduction band bottom [24–26]. The concentration of structural defects may be higher at the AE faces [27]. The interaction of structural defects with Ho^{3+} ions excited to high energy levels (as a result of upconversion processes taking place at high pump power densities) may lead to the appearance of electrons at the energy levels of defects and their subsequent thermally induced transition to the conduction band.

The existence of defects in ZrO_2–Y_2O_3(13.4 mol%)–Ho_2O_3(0.6 mol%) crystals is indicated by the band observed in the region of 254 nm in the luminescence excitation spectrum recorded at a Ho^{3+} luminescence wavelength of 541 nm (Fig. 11).

The interaction of Ho^{3+} ions in ZrO_2–Y_2O_3(13.4 mol%)–Ho_2O_3(0.6 mol%) crystals under laser excitation at a wavelength 1940 nm to the $^5I_7$ level is testified by the spectra of upconversion luminescence corresponding to the $^5I_6 \rightarrow {}^5I_8$ transition of Ho^{3+} ions (Fig. 12).

The second reason for burns can be self-focusing of radiation due to a high third-order nonlinearity typical for ZrO_2–Y_2O_3 crystals, which was experimentally and theoretically studied in [28].

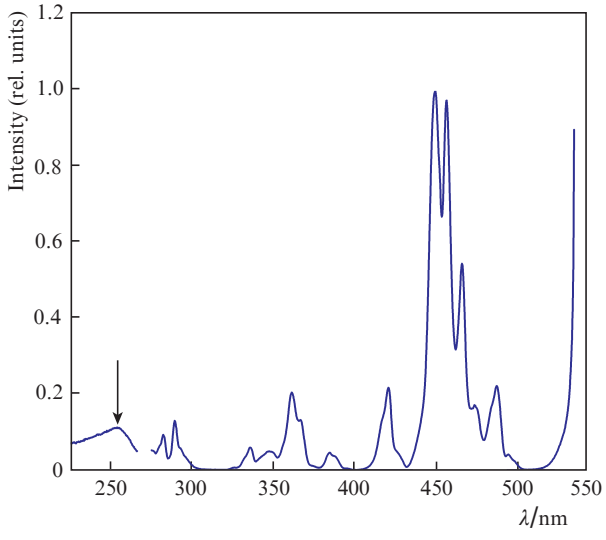

Figure 11. Luminescence excitation spectrum of ZrO_2–Y_2O_3 (13.4 mol%)–Ho_2O_3(0.6 mol%) crystals; λ_{reg} = 541 nm; T = 300 K.

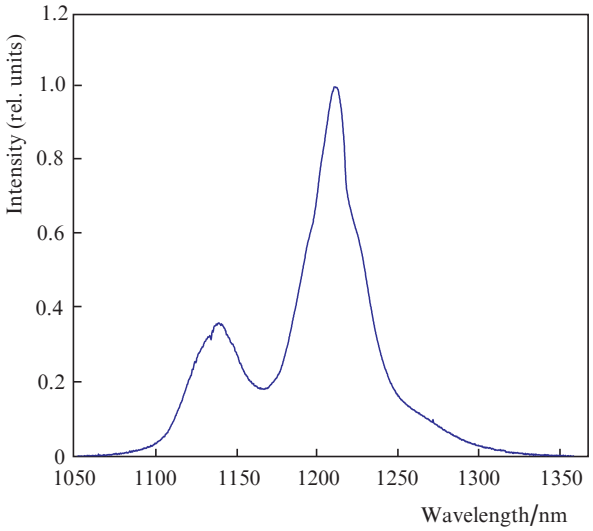

Figure 12. Luminescence spectrum of the $^5I_6 \rightarrow {}^5I_8$ transition of Ho^{3+} ions in the ZrO_2–Y_2O_3 (13.4 mol %)–Ho_2O_3(0.6 mol%) crystal in the case of excitation to the $^5I_7$ level; T = 300 K.

4. Conclusions

In this work, we have studied the parameters of *Q*-switched lasing in active elements that were made of ZrO_2–Y_2O_3(13.4 mol%)–Ho_2O_3(0.6 mol%) crystals grown with rates of 4 or 10 mm/h and whose faces were chemically and mechanically polished.

The experiments showed that the faces of all active elements have burns appearing with increasing laser power densities and decreasing laser pulse durations. This can be caused by both structural defects and self-focusing due to high third-order nonlinear optical susceptibilities of these crystals.

Acknowledgements. This work was supported by the Russian Foundation for Basic Research (Grant No. 18-29-20039). The authors thank M.V. Gerasimov for his help in taking photographs from a Carl Zeiss Axio Imager Z2 Vario high-resolution optical microscope.

References

1. Honea E.C., Beach R.J., Sutton S.B., Speth J.A., Mitchell S.C., Skidmore J.A., Emanuel M.A., Payne S.A. *IEEE J. Quantum Electron.*, **33**, 9 (1997).
2. Walsh B.M. *Laser Phys.*, **19**, 855 (2009).
3. Scholle K., Lamrini S., Koopmann P., Fuhrberg P., in *Frontiers in Guided Wave Optics and Optoelectronics* (Croatia: INTECH, 2010) p. 471.
4. Koopmann P., Peters R., Petermann K., Huber G. *Appl. Phys. B*, **102**, 1 (2011).
5. Koopmann P. *Long Wavelength Laser Operation of Tm: Sc_2O_3 at 2116 nm and Beyond* (OSA, 2011) paper ATuA5.
6. Antipov O.L., Novikov A.A., Zakharov N.G., Zinoviev A.P. *Opt. Mater. Express*, **2**, 183 (2012).
7. Lagatsky A.A., Fusari F., Kurilchik S.V., Kisel V.E., Yasukevich A.S., Kuleshov N.V., Pavlyuk A.A., Brown C.T.A., Sibbett W. *Appl. Phys. B*, **97** (2), 321 (2009).
8. Guo W., Chen Y., Lin Y., Gong X., Luo Z., Huang Y. *J. Phys. D: Appl. Phys.*, **41**, 115409 (2008).
9. Bol'shchikov F.A., Zharikov E.V., Zakharov N.G., Lis D.A., Ryabochkina P.A., Subbotin K.A., Antipov O.L. *Quantum Electron.*, **40**, 101 (2010) [*Kvantovaya Elektron.*, **40**, 101 (2010)].

10. Bol'shchikov F.A., Zharikov E.V., Zakharov N.G., Lis D.A., Ryabochkina P.A., Subbotin K.A., Antipov O.L. *Quantum Electron*., **40**, 847 (2010) [*Kvantovaya Elektron*., **40**, 847 (2010)].
11. Lyapin A.A., Fedorov P.P., Garibin E.A., Malov A.V., Osiko V.V., Ryabochkina P.A., Ushakov S.N. *Opt. Mater*., **35**, 1859 (2013).
12. Ryabochkina P.A., Chabushkin A.N., Kopylov Yu.L., Balashov V.V., Lopukhin K.V. *Quantum Electron*., **46**, 597 (2016) [*Kvantovaya Elektron*., **46**, 597 (2016)].
13. Antipov O.L., Novikov A.A., Larin S., Obronov I. *Opt. Lett*., **41**, 2298 (2016).
14. Wei Z., Haitao H., Xiang C., Jingru W., Rui X., Haotian W., Yongguang Z., Dingyuan T., Yishan W., Deyuan S. *Laser Phys*., **29**, 4 (2019).
15. Fei W., Jinwen T., Enhao L., Chongfeng S., Jun W., Dingyuan T., Deyuan S. *Opt. Lett*., **44**, 24 (2019).
16. Haolin Y., Yue C., Fuqiang J., Pengfei W. *Laser & Optoelectron. Progress*, **57**, 7 (2020).
17. Borik M.A., Lomonova E.E., Malov A.V., Kulebyakin A.V., Ryabochkina P.A., Ushakov S.N., Uslamina M.A., Chabushkin A.N. *Quantum Electron*., **42**, 580 (2012) [*Kvantovaya Elektron*., **42**, 580 (2012)].
18. Borik M.A., Lomonova E.E., Lyapin A.A., Kulebyakin A.V., Ryabochkina P.A., Ushakov S.N., Chabushkin A.N. *Quantum Electron*., **43**, 838 (2013) [*Kvantovaya Elektron*., **43**, 838 (2013)].
19. Ryabochkina P.A., Chabushkin A.N., Lyapin A.A., Lomonova E.E., Zakharov N.G., Vorontsov K.V. *Laser Phys. Lett*., **14**, 055807 (2017).
20. Chabushkin A.N., Lyapin A.A., Ryabochkina P.A., Antipov S.A., Lomonova E.E. *Laser Phys*., **28**, 3 (2018).
21. Ryabochkina P.A., Artemov S.A., Zakharov N.G., Saltykov E.V., Vorontsov K.V., Chabushkin A.N., Lomonova E.E. *Quantum Electron*., **50**, 8 (2020) [*Kvantovaya Elektron*., **50**, 8 (2020)].
22. Osiko V.V., Borik M.A., Lomonova E.E., Dhanaraj G., Byrappa K., Prasad V., Dudley M., in *Springer Handbook of Crystal Growth* (Berlin, 2010) pp 433 – 477.
23. Artemov S.A., Borik M.A., Volkova T.V., Gerasimov M.V., Kulebyakin A.V., Lomonova E.E., Milovich F.O., Myzina V.A, Ryabochkina P.A., Tabachkova N.Yu. *Opt. Mater*., **99**, 109611 (2020).
24. Merino R.I., Orera V.M., Povilla O., Assmus W., Lomonova E.E. *J. Phys. Chem. Solids*, **58**, 10 (1997).
25. Merino R.I., Orera V.M., Lomonova E.E., Batygov S.K. *Phys. Rev. B*, **52**, 9 (1995).
26. Aleksandrov V.I., Batygov S.Kh., Vishnyakova M.A., Voron'ko Yu.K., Kalabukhova V.F., Lavrishchev S.V., Lomonova E.E., Myzina V.A., Osiko V.V. *Fiz. Terd. Tela*, **26**, 5 (1984).
27. Yuanyuan L., Yasuo I., Browning N.D., Mazanec T. *J. Am. Ceram. Soc*., **85**, 9 (2002).
28. Marcaud G., Serna S., Karamanis P., Alonso-Ramos C., Le Roux X., Berciano M., Maroutian T., Agnus G., Aubert P., Jollivet A., Ruiz-Caridad A., Largeau L., Isac N., Cassan E., Matzen S., Dubreuil N., Rérat M., Philippe Lecoeur P., Vivien L. *Photonics Res.*, **8**, 110 (2020).